Synthesis, structure and high methane storage of pure D6R Yb(Y) nonanuclear cluster-based zeolite-like metal-organic frameworks

Hong-Xin Li,[a] Zong-Hui Zhang,[a] Han Fang,[a] Dong-Xu Xue,*[a] Junfeng Bai*[a]

[a] Key Laboratory of Applied Surface and Colloid Chemistry, Ministry of Education, Xi'an Key Laboratory of Organometallic Material Chemistry, School of Chemistry & Chemical Engineering, Shaanxi Normal University, Xi'an 710062, China.
E-mail: xuedx@snnu.edu.cn, bjunfeng@snnu.edu.cn.

Table of Contents

1. Materials and general procedures

All reagents were obtained from commercial sources and used without further purification. PXRD measurements were performed on a Bruker D8 Advance diffractometer with Cu *Kα* (λ = 1.5406 Å), and the X-ray tube was operated at 40 kV and 40 mA. High-resolution thermogravimetric analysis (TGA) was performed under a continuous N_2 flow and recorded on a Q600SDT thermal analyzer with a heating rate of 5 °C/min. Elemental analyses (C, H, and N) were obtained from a Vario EL cube analyzer. Fourier transform infrared (FT-IR) spectrum (400-4000 cm^{-1}, KBr pellet) was collected in the solid state on a Bruker Tensor 27 FT-IR spectrometer.

Synthesis of Yb-ZMOF-1

A mixture of $Yb(NO_3)_3 \cdot 6H_2O$ (40.6 mg, 0.087 mmol), H_2TZDB (13.5 mg, 0.0435 mmol), DMF (2.8 mL) and 2-FBA (FBA = 2-fluorobenzoic acid, 0.20 mL, 3.48 M/DMF) were combined in a 20 mL scintillation vial, sealed and heated to 120 °C for 48 h. The colourless spindly crystals were collected, washed with DMF, and then air-dried. Yield ≈ 89.6% (based on ligand). Selected IR (KBr, cm^{-1}): 3424 (br), 2928 (w), 1661 (vs), 1604 (s), 1549 (s), 1413 (vs), 1101 (m), 983 (m), 867 (m), 799 (m), 747 (m), 668 (w), 547 (m). Elem. Anal. (%) Calcd for: $C_{113}H_{125}F_{15}N_{25}O_{35}Yb_9$: C, 32.04; H, 2.97; N, 8.27. Found: C, 32.46; H, 3.20; N, 7.61.

Synthesis of Y-ZMOF-1

Similar procedures as synthesizing Yb-ZMOF-1 except that the rare-earth was substituted by $Y(NO_3)_3 \cdot 6H_2O$. Yield ≈ 86.3% (based on ligand). Selected IR (KBr, cm^{-1}): 3485 (br), 2935 (w), 1663 (vs), 1604 (m), 1555 (m), 1414 (vs), 1253 (m), 1099 (m), 986 (m), 873 (m), 798 (m), 749 (s), 667 (m), 551 (m). Elem. Anal. (%) Calcd for $C_{104}H_{112}F_{15}N_{22}O_{36}Y_9$: C, 37.50; H, 3.39; N, 9.25. Found: C, 37.82; H, 3.97; N, 9.09.

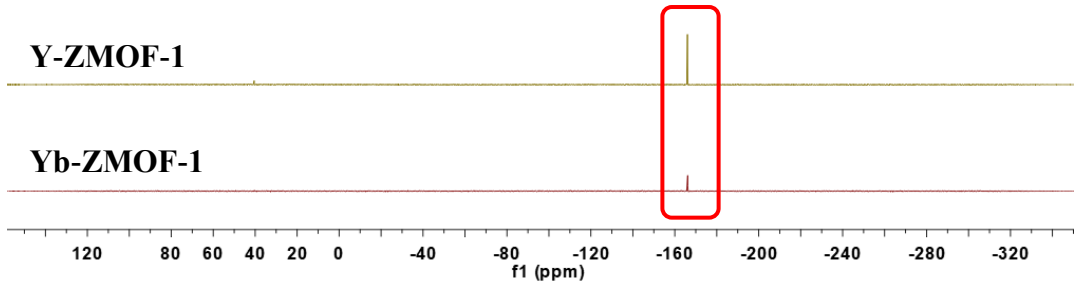

Fig. S1 The ^{19}F NMR (400 MHz, DMSO-d_6) spectra of Yb-ZMOF-1 and Y-ZMOF-1. For both materials, there is a small peak at δ = -166 ppm. This signal is attributed to HF, from the dissolved materials in H_2SO_4 and DMSO-d_6.

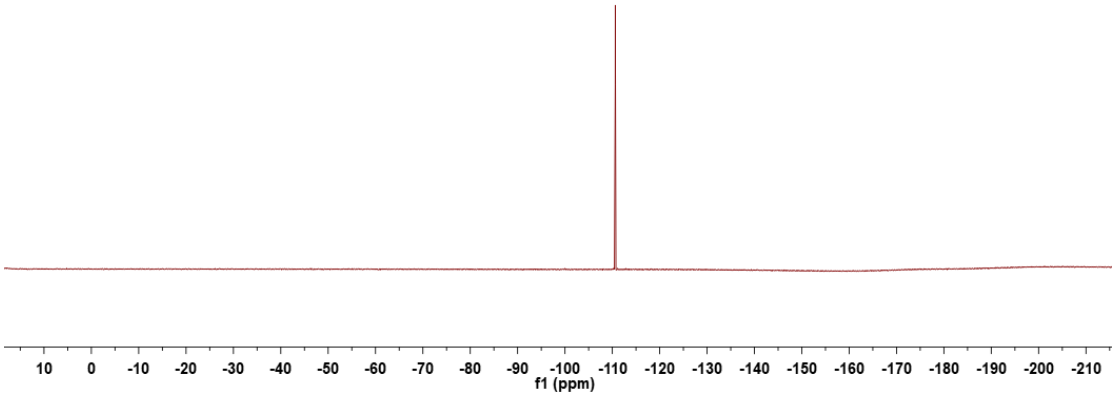

Fig. S2 The ^{19}F NMR (400 MHz, DMSO-d_6) spectra of 2-fluorobenzoic acid, it has a peak at δ = -110 ppm.

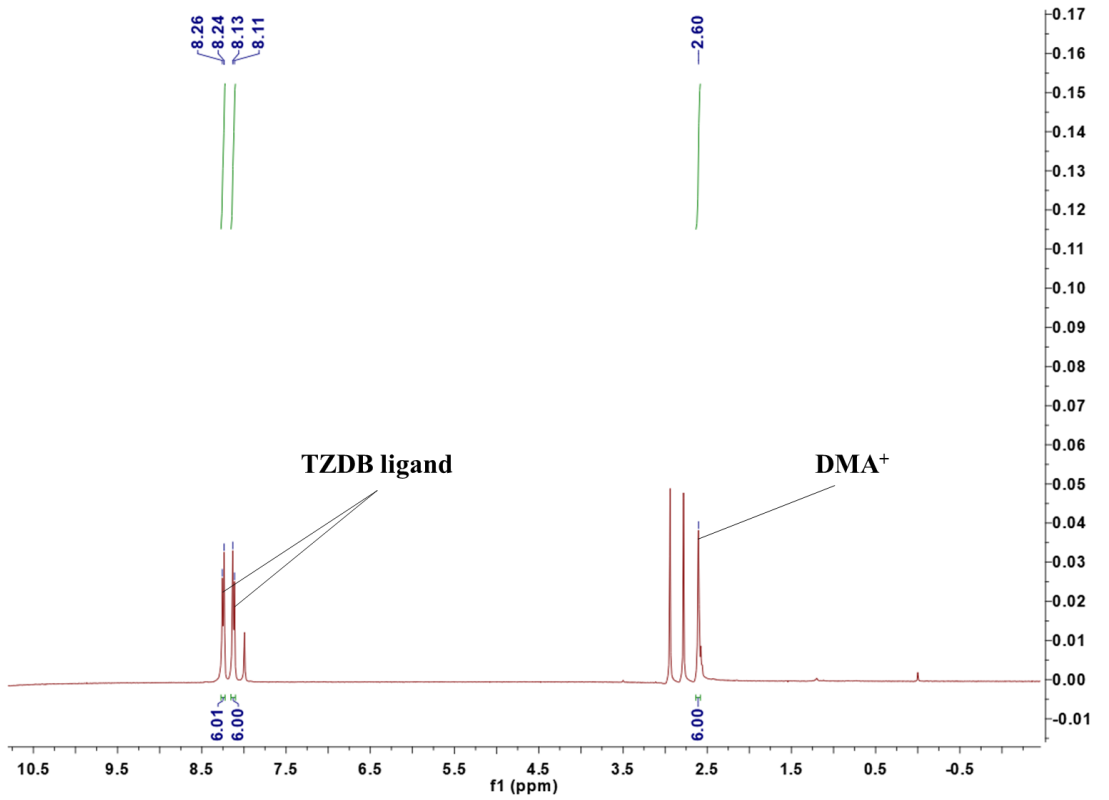

Fig. S3 The ^{1}H NMR (400 MHz, DMSO-d_6) spectra of acid digested as-synthesized Yb-ZMOF-1 samples, the ratio between TZDB and DMA^{+} inside this ZMOF is 3:2.

2. Additional structural figures

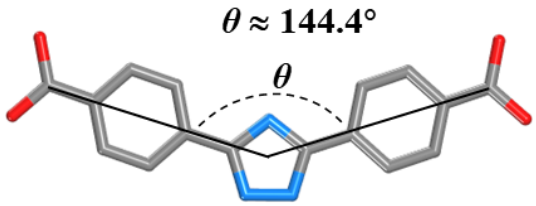

Fig. S4 Representation of the angular ligand within Yb-ZMOF-1.

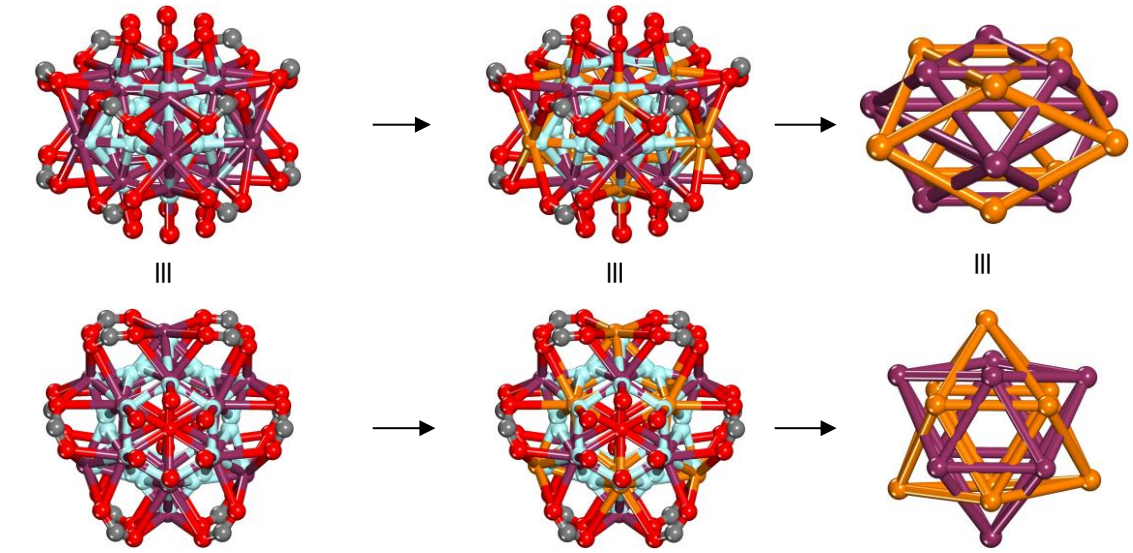

Fig. S5 Directly observed disorder cluster in Yb-ZMOF-1, Yb = purple/orange, C = gray, O = red and F = cyan.

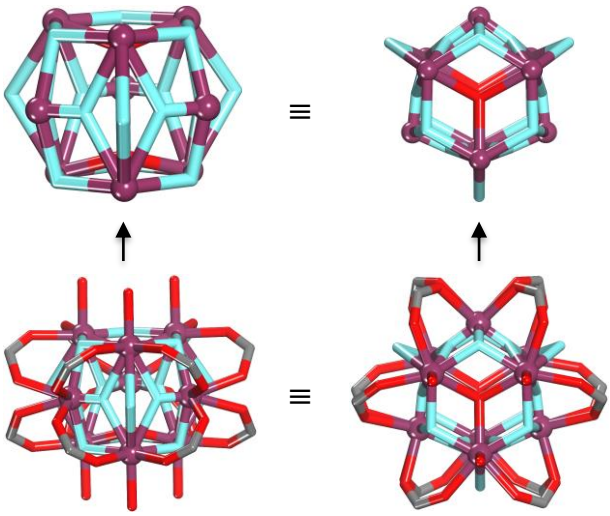

Fig. S6 Schematic representation of the unique nonanuclear MBB of $[Yb_9(\mu_3\text{-}F)_{12}(\mu_2\text{-}F)_3(\mu_3\text{-}O)_2(O_2C\text{–})_{12}(H_2O)_6]$ in Yb-ZMOF-1. Yb = purple, C = gray, O = red and F = cyan.

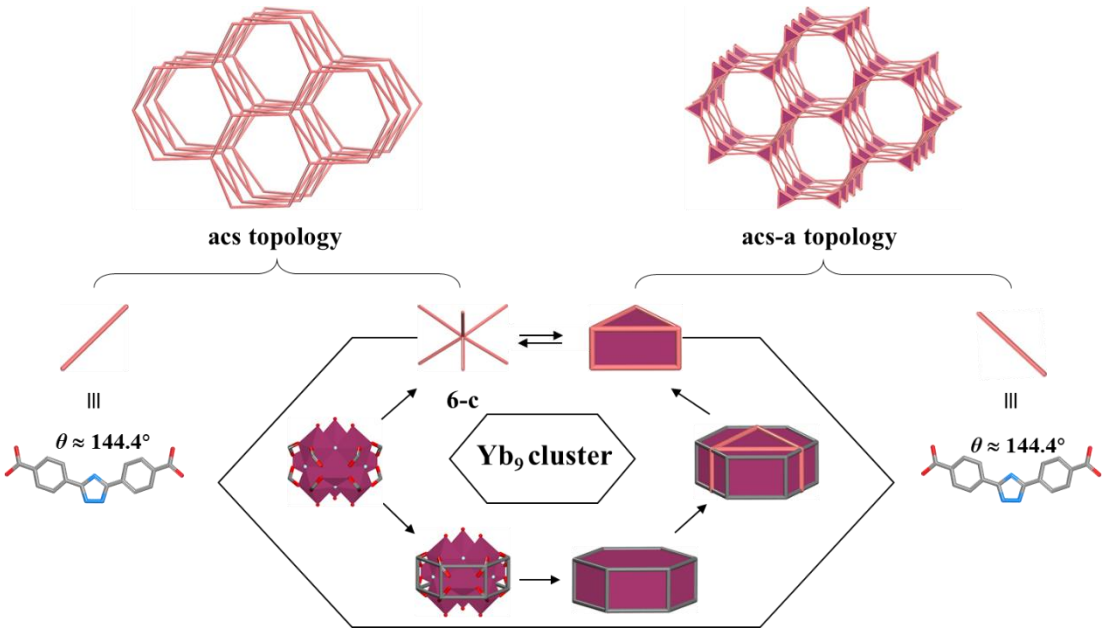

Fig. S7 Schematic representation of the simplified process of Yb_9 cluster within Yb-ZMOF-1, and the corresponding **acs** net in node−linker and augmented forms, respectively.

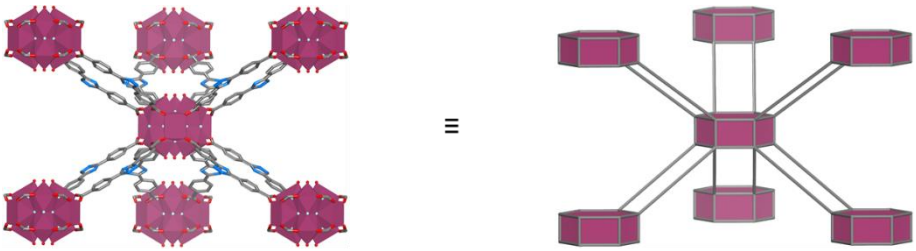

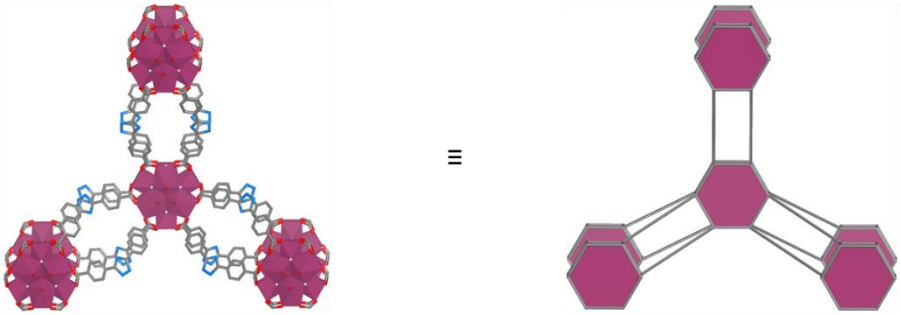

Fig. S8 The connecting environment of Yb_9 cluster within Yb-ZMOF-1 in different views.

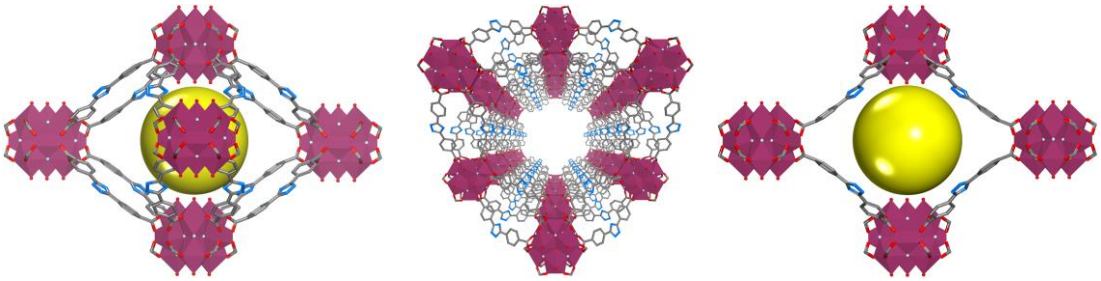

gme cage: 11.1 × 20.4 Å² **Channel: 18.4 Å** **Window:12.8 Å**

Fig. S9 Schematic representation of gme cage, one channel, as well as one window and their sizes in Yb/Y-ZMOF-1.

3. Powder X-ray Diffraction (PXRD) patterns

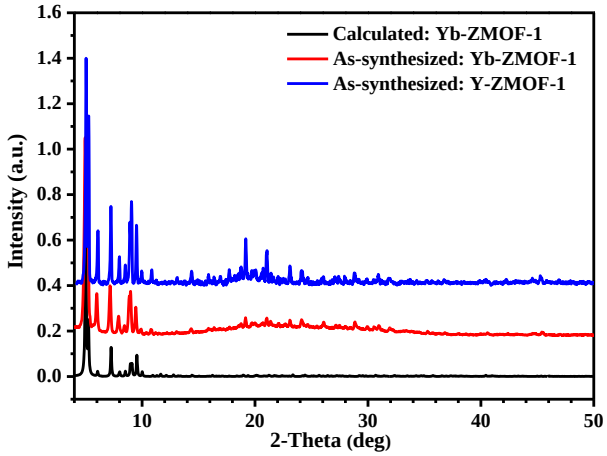

Fig. S10 PXRD patterns of Yb-ZMOF-1 and Y-ZMOF-1.

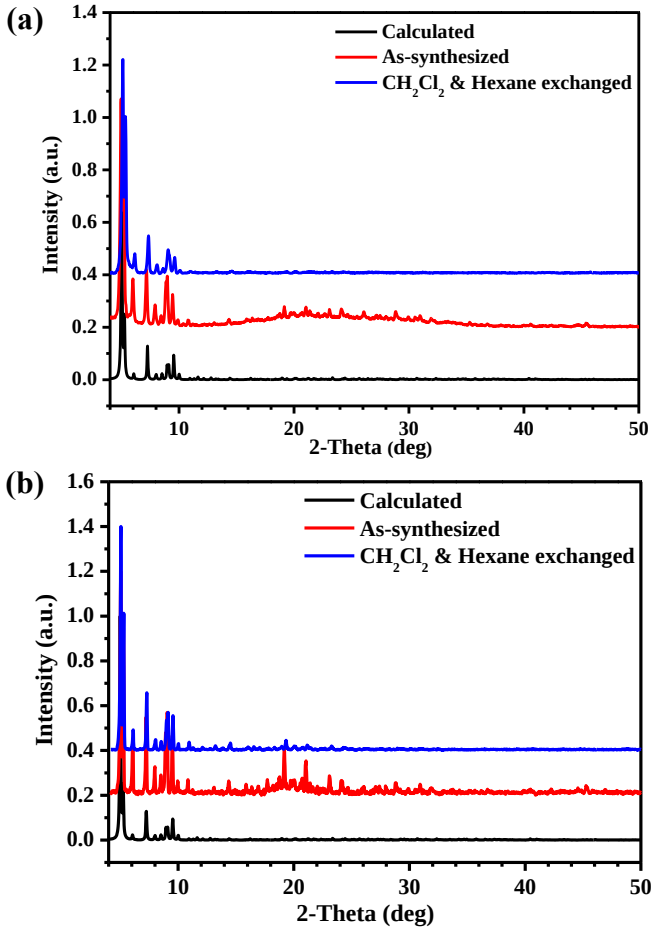

Fig. S11 PXRD patterns of (a) Yb-ZMOF-1 and (b) Y-ZMOF-1 after different treatments.

4. Thermal Gravimetric Analysis (TGA)

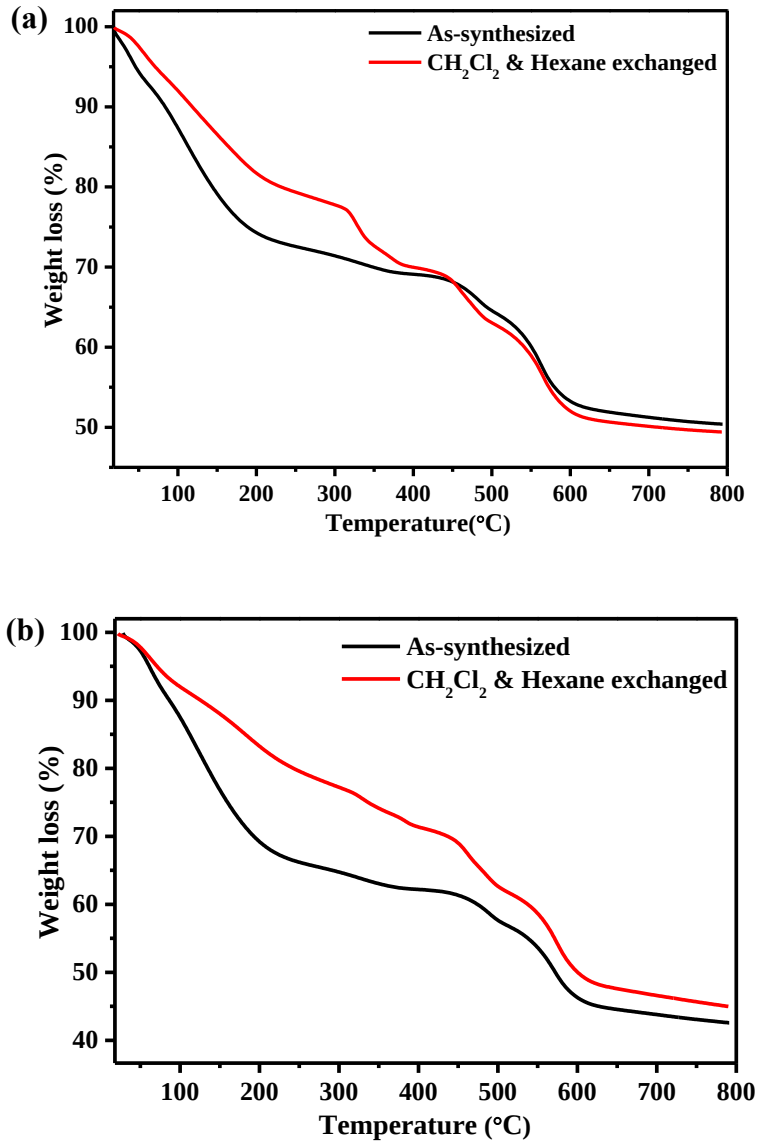

Fig. S12 TGA plots of the as-synthesized and solvent-exchanged (a) Yb-ZMOF-1 and (b) Y-ZMOF-1.

5. Low-pressure gas sorption measurements

Low pressure gas sorption studies were conducted on a fully automated micropore gas analyzer Autosorb-iQ3 (Quantachrome Instruments) at relative pressures up to 1 atm. The cryogenic temperature was controlled using liquid nitrogen at 77 K. The apparent surface areas were determined from the nitrogen adsorption isotherms collected at 77 K by applying the BET models. Pore size analyses were performed using a cylindrical/spherical NLDFT pore model system by assuming an oxidic (zeolitic) surface.

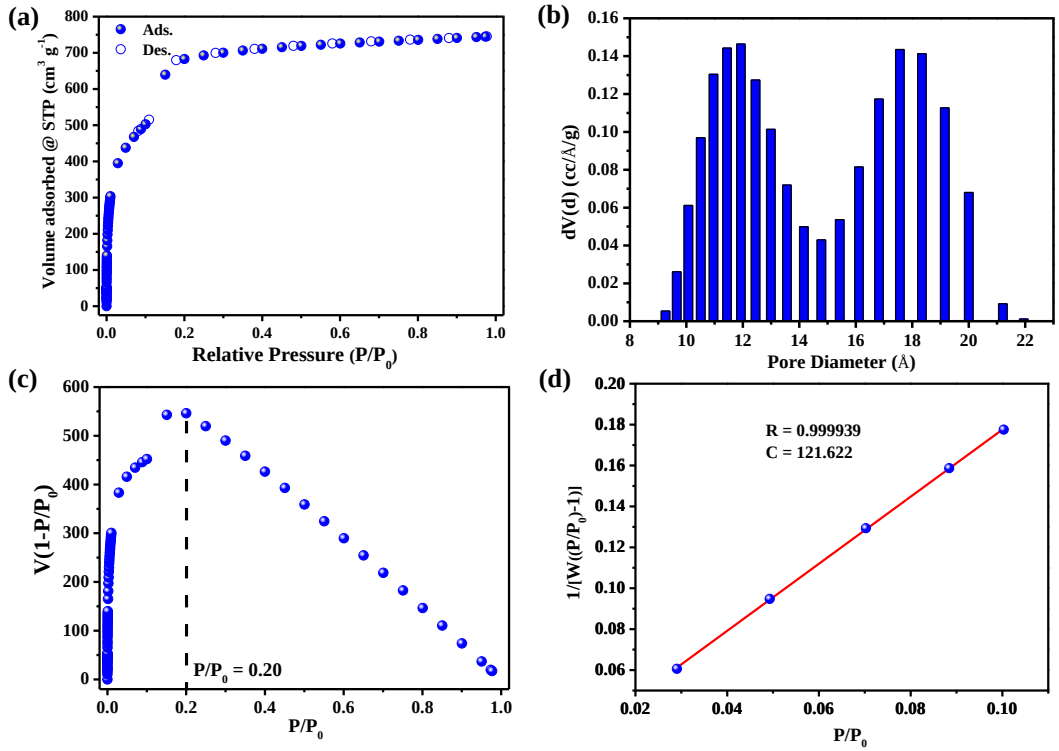

Fig. S13 (a) Adsorption (closed) / desorption (open) isotherms and (b) pore size distribution of Yb-ZMOF-1, (c) $V(1-P/P_0)$ vs. P/P_0 for Yb-ZMOF-1. Only the range below $P/P_0 = 0.20$ satisfies the first consistency criterion for applying the BET theory and (d) plot of the linear region for the BET equation.

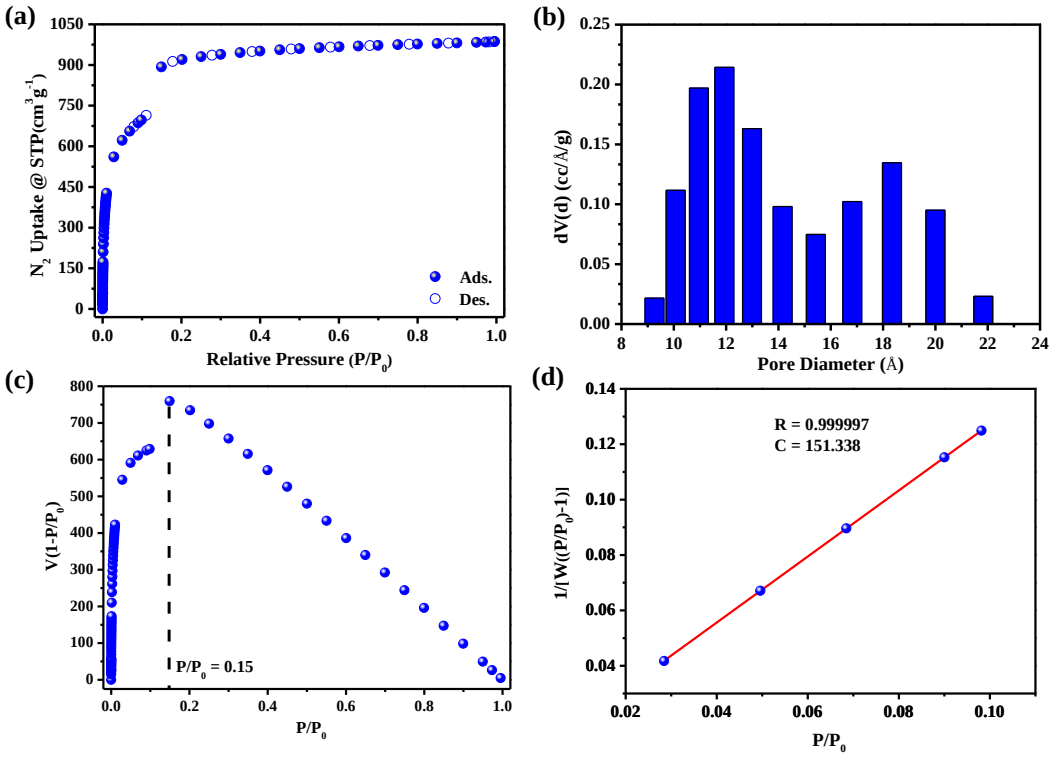

Fig. S14 (a) Adsorption (closed) / desorption (open) isotherms and (b) pore size distribution of Y-ZMOF-1, (c) $V(1-P/P_0)$ vs. P/P_0 for Y-ZMOF-1. Only the range below $P/P_0 = 0.15$ satisfies the first consistency criterion for applying the BET theory and (d) plot of the linear region for the BET equation.

Table S1. The BET surface areas summary of investigated ZMOFs.

Materials	Net	BET ($m^2 g^{-1}$)	Ref.
$[\{Zn(mim)_2 \cdot 2H_2O\}_\infty]$	**sod**	1030	1
$[\{Zn(eim)_2 \cdot H_2O\}_\infty]$	**ana**	28.7	
$[\{Zn(eim/mim)_2 \cdot 1.25H_2O\}_\infty]$	**rho**	–	
$[Pd(2\text{-}pymo)_2]_n$	**sod**	600	2
$[Cu(2\text{-}pymo)_2]_n$	**sod**	350	
$[Cu(4\text{-}pymo)_2]_n$	**sod**	65	
$\{[Zn(btz)] \cdot DMF \cdot 0.5H_2O\}_n$	**sod**	1151	3
IFMC-1	**sod**	780	4
ZIF-8	**sod**	1630	5
ZIF-11	**rho**	–	
ZIF-95	**poz**	1050	6
ZIF-100	**moz**	595	
ZIF-68	**gme**	1090	7
ZIF-69	**gme**	950	
ZIF-70	**gme**	1730	
ZIF-78	**gme**	620	
ZIF-79	**gme**	810	
ZIF-81	**gme**	760	
ZIF-82	**gme**	1300	
ZIF-93	**rho**	864	8
ZIF-94	**sod**	480	
ZIF-25	**rho**	1110	9
ZIF-71	**rho**	652	
ZIF-96	**rho**	960	
ZIF-97	**rho**	564	
ZIF-300	**cha**	420	10
ZIF-301	**cha**	680	
ZIF-302	**cha**	240	
ZIF-303	**cha**	–	11
ZIF-360	**kfi**	1050	
ZIF-365	**kfi**	920	
ZIF-376	**lta**	–	
ZIF-386	**afx**	740	
ZIF-408	**moz**	–	
ZIF-410	**gme**	800	
ZIF-486	**gme**	1180	
ZIF-412	**ucb**	1520	
ZIF-413	**ucb**	1290	
ZIF-414	**ucb**	1440	
ZIF-516	**ykh**	640	

ZIF-586	**ykh**	–	
ZIF-615	**gcc**	770	
ZIF-725	**bam**	720	
TIF1-Zn	**zea**	667.5($S_{Langmuir}$)	12
TIF-2	**zeb**	618.2($S_{Langmuir}$)	13
BIF-3-Cu	**sod**	182.3($S_{Langmuir}$)	14
BIF-3-Li	**sod**	726.5($S_{Langmuir}$)	
MIL-101c	**mtn**	4230	15, 16
MIL-100	**mtn**	3100	17
rho-ZMOF	**rho**	1067	18
sod-ZMOF	**sod**	–	
$[Tb_{16}(TATB)_{16}(DMA)_{24}]\cdot(DMA)_{91}(H_2O)_{108}$	**mtn**	1783	19
$[Cd(pymc)_2]\cdot 7H_2O$	**rho**	804($S_{Langmuir}$)	20
usf-ZMOF	**med**	520($S_{Langmuir}$)	21
ZSA-1	**gis**	1382	22
ZSA-2	**rho**	395	
$Li_4(OPy)_4$	**aco**	440.3	23
$(Et_2NH_2)[In(BCBAIP)]\cdot 4DEF\cdot 4EtOH$	**sod**	209	24
PCN-777	**β-cristobalite**	2008	25
JLU-Liu23	**unj**	584	26
Y-kex-MOF-1	**afx**	1580	27
ZSA-10	**mer**	724	28
ZSA-11	**abw**	–	
Zr-sod-ZMOF-1	**sod**	1565	29
Zr-sod-ZMOF-2	**sod**	–	
Yb-ZMOF-1	**gme**	**2107**	**This work**
Y-ZMOF-1	**gme**	**2902**	

6. High-pressure gas sorption measurements

High-pressure excess gas sorption isotherms were measured with an automatic volumetric sorption apparatus (BELSORP-HP) in the range of 0–80 bar. The bath temperature for CH_4 sorption measurements was controlled using a recirculating bath containing an ethylene glycol/H_2O mixture. Ultrahigh purity He was used to determine the dead space of the sample cell. The adsorption data were corrected to give the final gravimetric excess adsorption isotherm n_{ex} (P, T), by subtracting the background adsorption measured with the empty sample cell using the same test parameters. The total sorption, which represents the real gas-storage performance of the porous material but cannot be directly measured, was calculated by [Eqn. (1)]:

$$n_{tot}(P, T) = n_{ex}(P, T) + \rho_{gas}(P, T) \times V_P \quad (1)$$

Where ρ_{gas} (P, T) is the density of bulk methane at pressure P and temperature T, and V_p is the pore volume of the porous material determined from N_2 adsorption isotherm at 77 K.

The isosteric enthalpy of adsorption, Q_{st} for CH_4 was determined by fitting the adsorption isotherms at 298 and 273 K to the Dual-site Langmuir equation (Eqn 2);

$$n = \frac{n_{L,A} b_A p}{1 + b_A p} + \frac{n_{L,B} b_B p}{1 + b_B p} \quad (2)$$

Where n is the amount of gas adsorbed in mmol/g, P is the pressure in Pa, $n_{L,A}$ and $n_{L,B}$ are the saturation capacity in mmol/g, and b_A *and* b_B are the Langmuir parameter up to two sites 1 and 2.

Using the Dual-site Langmuir fit, the isosteric heat of adsorption can be calculated for each material as a function of the total amount of CH_4 adsorbed using the Clausius-Clapeyron relation (Eqn 3).

$$\frac{dlnp}{dT} = \frac{\Delta H}{nRT^2} = \frac{\Delta_r H_m}{RT^2} \quad (3)$$

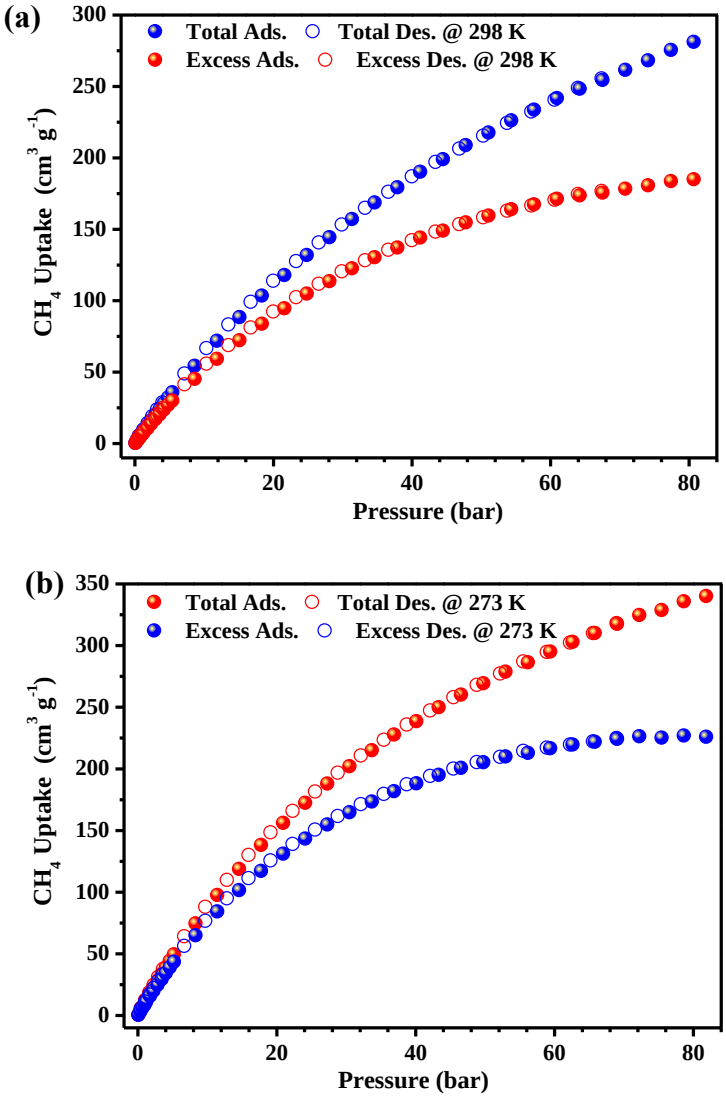

Fig. S15 High-pressure methane adsorption (closed) / desorption (open) isotherms of Yb-ZMOF-1.

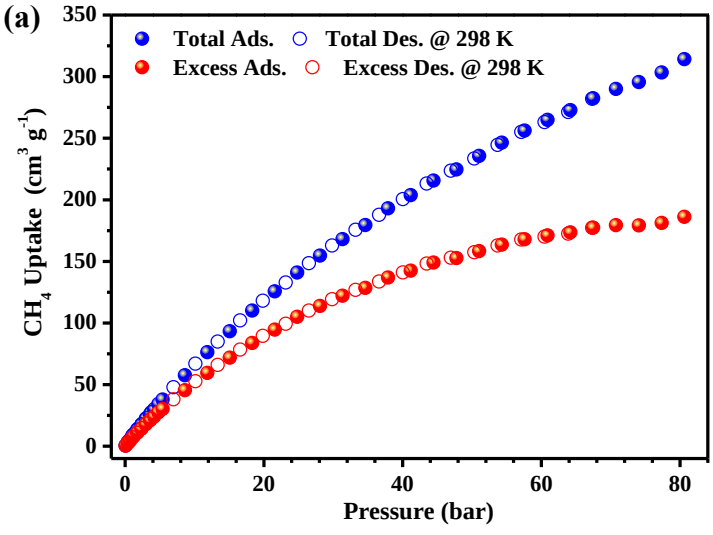

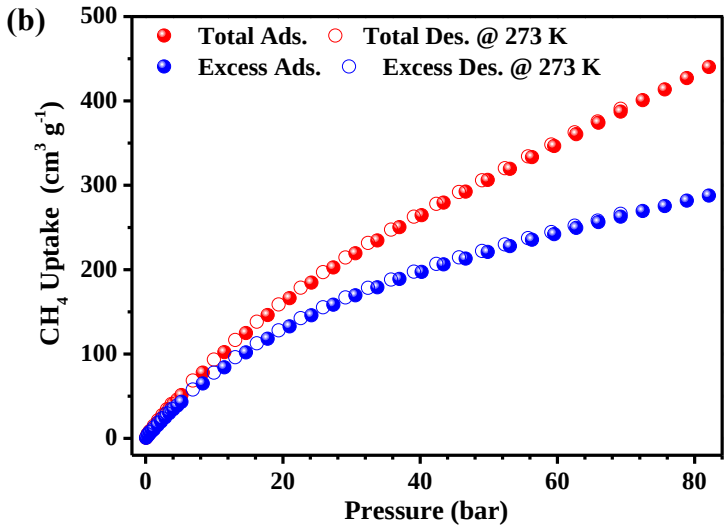

Fig. S16 High-pressure methane adsorption (closed) / desorption (open) isotherms of Y-ZMOF-1.

Table S2. The methane adsorption data summary of Yb-ZMOF-1 and Y-ZMOF-1.

Name	BET ($m^2\ g^{-1}$)	V_p ($cm^3\ g^{-1}$)	ρ ($g\ cm^{-3}$)	T (K)	Uptake ($cm^3\ g^{-1}$) 5 / 65 / 80 bar	Working capacity ($cm^3\ g^{-1}$) 5 - 65 / 80 bar	Uptake ($cm^3\ cm^{-3}$) 5 / 65 / 80 bar	Working capacity ($cm^3\ cm^{-3}$) 5 – 65 / 80 bar	Uptake ($g\ g^{-1}$) 5 / 65 / 80 bar	Working capacity ($g\ g^{-1}$) 5 - 65 / 80 bar	Q_{st} ($kJ\ mol^{-1}$)
Yb-ZMOF-1	2107	1.15	0.585640	298	34 / 250 / 281	216 / 247	20 / 147 / 164	127 / 144	0.02 / 0.18 / 0.20	0.16 / 0.18	9.5
				273	48 / 309 / 339	261 / 291	28 / 181 / 198	153 / 170	0.03 / 0.22 / 0.24	0.19 / 0.21	
Y-ZMOF-1	2902	1.53	0.469552	298	36 / 275 / 313	239 / 277	17 / 129 / 147	112 / 130	0.03 / 0.20 / 0.22	0.17 / 0.19	8.5
				273	50 / 370 / 432	320 / 382	23 / 174 / 203	151 / 180	0.04 / 0.27 / 0.31	0.23 / 0.27	

Table S3. Experimental methane deliverable capacities of the investigated MOFs.

MOF	T/K	Working capacity 5-80 bar ($g\ g^{-1}$)	Ref.
ST-2	273	0.43	30
Al-soc-MOF-1	273	0.5	31
NU-1500-Al	270	0.3	32
Ni-MOF-74	273	0.08	33
HKUST-1	273	0.15	33
Yb-ZMOF-1	273	0.21	This work
Y-ZMOF-1	273	0.27	

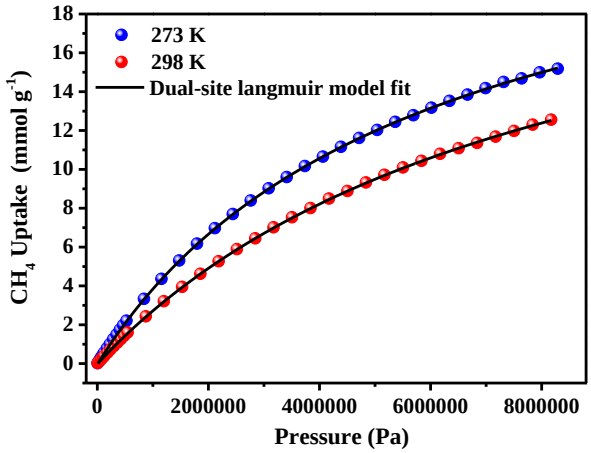

Fig. S17 Dual-site Langmuir model fitting (lines) of CH_4 adsorption isotherms (points) for Yb-ZMOF-1 measured at 273 and 298 K.

Table S4. The obtained Dual-site Langmuir model fitting parameters for Yb-ZMOF-1.

T (K)	$n_{L,A}$	$n_{L,B}$	b_A	b_B	R^2
273	0.772443	2.53006	6.53704E-7	1.64018E-7	0.999989
298	25.1521	0.0390026	1.20785E-7	6.45643E-6	0.999986

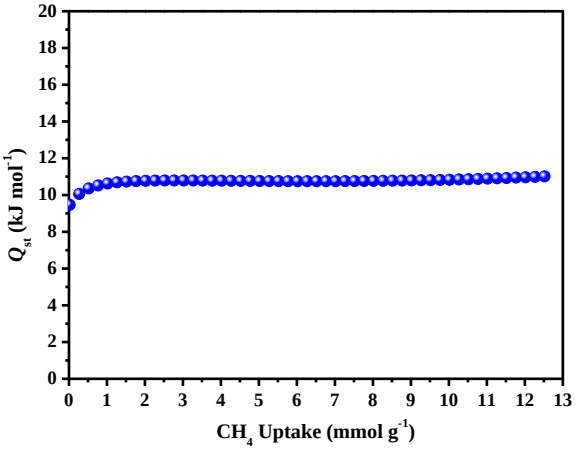

Fig. S18 Heats of CH_4 adsorption (Q_{st}) for Yb-ZMOF-1, which were calculated from the Dual-site Langmuir model fitting of adsorption isotherms at 273 and 298 K as a function of the total CH_4 uptake amount using the Clausius-Clapeyron equation: $\frac{dlnp}{dT} = \frac{\Delta H}{nRT^2} = \frac{\Delta_r H_m}{RT^2}$.

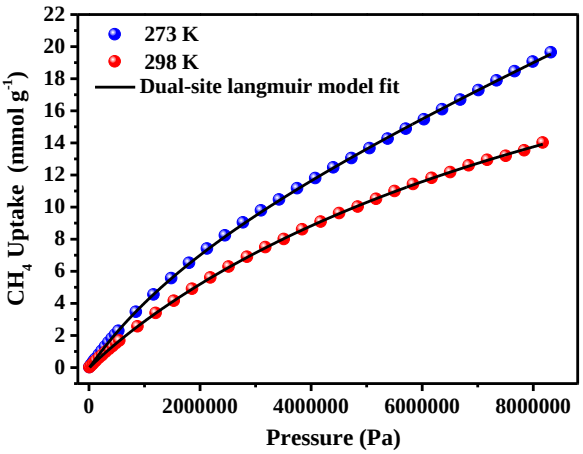

Fig. S19 Dual-site Langmuir model fitting (lines) of CH_4 adsorption isotherms (points) for Y-ZMOF-1 measured at 273 and 298 K.

Table S5. The obtained Dual-site Langmuir model fitting parameters for Y-ZMOF-1.

T(K)	$n_{L,A}$	$n_{L,B}$	b_A	b_B	R^2
273	9.78632	3715.14	3.57963E-7	3.9704E-10	0.999941
298	0.509062	31.6332	1.20178E-6	9.07909E-8	0.999958

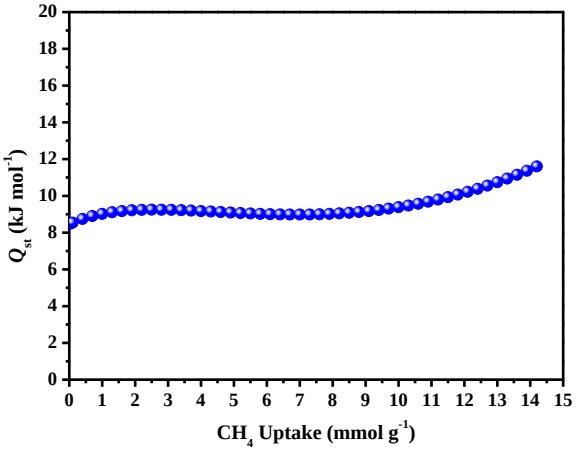

Fig. S20 Heats of CH_4 adsorption (Q_{st}) for Y-ZMOF-1, which were calculated from the Dual-site Langmuir model fitting of adsorption isotherms at 273 and 298 K as a function of the total CH_4 uptake amount using the Clausius-Clapeyron equation: $\frac{dlnp}{dT} = \frac{\Delta H}{nRT^2} = \frac{\Delta_r H_m}{RT^2}$.

7. Single Crystal X-ray Crystallography Data

Single-crystal X-ray diffraction data for Yb-ZMOF-1 were collected on a Bruker D8 venture diffractometer (Cu/$K\alpha$, λ = 1.54178 Å) at 153 K. Indexing was performed using APEX3 (Difference Vectors method).[34] Data integration and reduction were performed using SaintPlus 6.01.[35] Absorption correction was performed by multi-scan method implemented in SADABS.[36] Space group was determined using XPREP implemented in APEX3. The structure was solved by direct methods and refined with full-matrix least squares technique using the SHELXT[37] package or refined using SHELXL-2014 (full-matrix least-squares on F^2) contained in Olex2.[38] Non-hydrogen atoms were refined with anisotropic displacement parameters during the final cycles. Hydrogen atoms were located at geometrically calculated positions to their carrier atoms and refined with isotropic thermal parameters included in the final stage of the refinement. For this compound, the contributions of heavily disordered solvent molecules were treated as diffuse using Squeeze procedure implemented in Platon program.[39-41]

A summary of the crystallographic data is given in Table S6. CCDC 2163665 (Yb-ZMOF-1) contain the supplementary crystallographic data for this paper. The data can be obtained free of charge from The Cambridge Crystallographic Data Centre.

Table S6. Crystal data and refinement results for Yb-ZMOF-1.

Identification code	**Yb-ZMOF-1**
Empirical formula	C_{96} H_{60} F_{15} N_{18} O_{32} Yb_9
Formula weight	3819.98
Temperature/K	153.0
Wavelength/Å	1.54178
Crystal system	Hexagonal
Space group	$P6_3/mmc$
Unit cell dimensions/Å	a = 33.598(5) c = 22.159(4)
Volume/Å^3	21662.5(7)
Z	2
Density (calculated)/Mg/m^3	0.586
Absorption coefficient/mm^{-1}	3.674
F (000)	3566.0
Crystal size/mm^3	0.10 x 0.10 x 0.06
Theta range for data collection/°	2.506 to 50.682
Index ranges	-33<=h<=30 -26<=k<=33 -21<=l<=22
Reflections collected	66891
Independent reflections	4197 [R(int) = 0.2190]
Completeness to theta = 50.682°	99.3%
Refinement method	Full-matrix least-squares on F^2
Data / restraints / parameters	4197 / 294 / 164
Goodness-of-fit on F^2	0.936
Final R indices [I>2sigma(I)]	R_1 = 0.0820, wR_2 = 0.2370
R indices (all data)	R_1 = 0.1148, wR_2 = 0.2648
Largest diff. peak and hole/e.Å^{-3}	0.72 and -1.51

8. References

1. X. C. Huang, Y. Y. Lin, J. P. Zhang and X. M. Chen, *Angew. Chem., Int. Ed.*, 2006, **45**, 1557-1559.
2. J. A. R. Navarro, E. Barea, J. M. Salas, N. Masciocchi, S. Galli, A. Sironi, C. O. Ania and J. B. Parra, *Inorg. Chem.*, 2006, **45**, 2397-2399.
3. P. Cui, Y. G. Ma, H. H. Li, B. Zhao, J. R. Li, P. Cheng, P. B. Balbuena and H. C. Zhou, *J. Am. Chem. Soc.*, 2012, **134**, 18892-18895.
4. J.-S. Qin, D.-Y. Du, W.-L. Li, J.-P. Zhang, S.-L. Li, Z.-M. Su, X.-L. Wang, Q. Xu, K.-Z. Shao and Y.-Q. Lan, *Chem. Sci.*, 2012, **3**, 2114-2118.
5. K. S. Park, Z. Ni, A. P. Cote, J. Y. Choi, R. Huang, F. J. Uribe-Romo, H. K. Chae, M. O'Keeffe and O. M. Yaghi, *Proc. Natl. Acad. Sci. U.S.A.*, 2006, **103**, 10186-10191.
6. B. Wang, A. P. Cote, H. Furukawa, M. O'Keeffe and O. M. Yaghi, *Nature*, 2008, **453**, 207-211.
7. R. Banerjee, H. Furukawa, D. Britt, C. Knobler, M. O'Keeffe and O. M. Yaghi, *J. Am. Chem. Soc.*, 2009, **131**, 3875-3877.
8. W. Morris, N. He, K. G. Ray, P. Klonowski, H. Furukawa, I. N. Daniels, Y. A. Houndonougbo, M. Asta, O. M. Yaghi and B. B. Laird, *J. Phys. Chem. C*, 2012, **116**, 24084-24090.
9. Y. Houndonougbo, C. Signer, N. He, W. Morris, H. Furukawa, K. G. Ray, D. L. Olmsted, M. Asta, B. B. Laird and O. M. Yaghi, *J. Phys. Chem. C*, 2013, **117**, 10326-10335.
10. N. T. T. Nguyen, H. Furukawa, F. Gandara, H. T. Nguyen, K. E. Cordova and O. M. Yaghi, *Angew. Chem., Int. Ed.*, 2014, **53**, 10645-10648.
11. J. Yang, Y. B. Zhang, Q. Liu, C. A. Trickett, E. Gutierrez-Puebla, M. A. Monge, H. Cong, A. Aldossary, H. Deng and O. M. Yaghi, *J. Am. Chem. Soc.*, 2017, **139**, 6448-6455.
12. T. Wu, X. Bu, R. Liu, Z. Lin, J. Zhang and P. Feng, *Chem. Eur. J.*, 2008, **14**,

7771-7773.

13. T. Wu, X. Bu, J. Zhang and P. Feng, *Chem. Mater.*, 2008, **20**, 7377-7382.
14. J. Zhang, T. Wu, C. Zhou, S. Chen, P. Feng and X. Bu, *Angew. Chem., Int. Ed.*, 2009, **48**, 2542-2545.
15. G. Ferey, C. Mellot-Draznieks, C. Serre, F. Millange, J. Dutour, S. Surble and I. Margiolaki, *Science*, 2005, **309**, 2040-2042.
16. P. L. Llewellyn, S. Bourrelly, C. Serre, A. Vimont, M. Daturi, L. Hamon, G. De Weireld, J.-S. Chang, D.-Y. Hong, Y. K. Hwang, S. H. Jhung and G. Ferey, *Langmuir*, 2008, **24**, 7245-7250.
17. G. Ferey, C. Serre, C. Mellot-Draznieks, F. Millange, S. Surble, J. Dutour and I. Margiolaki, *Angew. Chem., Int. Ed.*, 2004, **43**, 6296-6301.
18. Y. Liu, V. Kravtsov, R. Larsen and M. Eddaoudi, *Chem. Commun.*, 2006, 1488-1490.
19. Y. K. Park, S. B. Choi, H. Kim, K. Kim, B.-H. Won, K. Choi, J.-S. Choi, W.-S. Ahn, N. Won, S. Kim, D. H. Jung, S.-H. Choi, G.-H. Kim, S.-S. Cha, Y. H. Jhon, J. K. Yang and J. Kim, *Angew. Chem., Int. Ed.*, 2007, **46**, 8230-8233.
20. J. Y. Zhang, A. L. Cheng, Q. Yue, W. W. Sun and E. Q. Gao, *Chem. Commun.*, 2008, 847-849.
21. Y. Liu, V. Kravtsov and M. Eddaoudi, *Angew. Chem., Int. Ed.*, 2008, **47**, 8446-8449.
22. S. Wang, T. Zhao, G. Li, L. Wojtas, Q. Huo, M. Eddaoudi and Y. Liu, *J. Am. Chem. Soc.*, 2010, **132**, 18038-18041.
23. X. Zhao, T. Wu, S.-T. Zheng, L. Wang, X. Bu and P. Feng, *Chem. Commun.*, 2011, **47**, 5536-5538.
24. L. Sun, H. Xing, Z. Liang, J. Yu and R. Xu, *Chem. Commun.*, 2013, **49**, 11155-11157.
25. D. Feng, K. Wang, J. Su, T. F. Liu, J. Park, Z. Wei, M. Bosch, A. Yakovenko, X. Zou and H. C. Zhou, *Angew. Chem., Int. Ed.*, 2015, **54**, 149-154.
26. X. Luo, Y. Cao, T. Wang, G. Li, J. Yon, Y. Yang, Z. Xu, J. Zhang, Q. Huo, Y. Liu and M. Eddaoudi, *J. Am. Chem. Soc.*, 2016, **138**, 786-789.

27. Z. Chen, Z. Thiam, A. Shkurenko, L. J. Weselinski, K. Adil, H. Jiang, D. Alezi, A. H. Assen, M. O'Keeffe and M. Eddaoudi, *J. Am. Chem. Soc.*, 2019, **141**, 20480-20489.
28. J. Li, L. Kan, J. Li, Y. Liu and M. Eddaoudi, *Angew. Chem., Int. Ed.*, 2020, **59**, 19659-19662.
29. N. Alsadun, G. Mouchaham, V. Guillerm, J. Czaban-Jozwiak, A. Shkurenko, H. Jiang, P. M. Bhatt, P. Parvatkar and M. Eddaoudi, *J. Am. Chem. Soc.*, 2020, **142**, 20547-20553.
30. C.-C. Liang, Z.-L. Shi, C.-T. He, J. Tang, H.-D. Zhou, H.-L. Zhou, Y. Lee and Y.-B. Zhang, *J. Am. Chem. Soc.*, 2017, **139**, 13300-13303.
31. D. Alezi, Y. Belmabkhout, M. Suyetin, P. M. Bhatt, L. J. Weselinski, V. Solovyeva, K. Adil, I. Spanopoulos, P. N. Trikalitis, A.-H. Emwas and M. Eddaoudi, *J. Am. Chem. Soc.*, 2015, **137**, 13308-13318.
32. Z. Chen, P. Li, R. Anderson, X. Wang, X. Zhang, L. Robison, L. R. Redfern, S. Moribe, T. Islamoglu, D. A. Gomez-Gualdron, T. Yildirim, J. F. Stoddart and O. K. Farha, *Science*, 2020, **368**, 297-303.
33. J. A. Mason, M. Veenstra and J. R. Long, *Chem. Sci.*, 2014, **5**, 32-51.
34. Bruker APEX2; Bruker AXS, Inc.: Madison, WI, 2010.
35. Bruker SAINT, Data Reduction Software; Bruker AXS, Inc.: Madison, WI, 2009.
36. G. M. Sheldrick, University of Gottingen: Gottingen, Germany, 1996.
37. G. M. Sheldrick, *Acta Crystallogr.*, 2015, **A71**, 3-8.
38. O. V. Dolomanov, L. J. Bourhis, R. J. Gildea, J. A. K. Howard, H. Puschmann, *J. Appl. Crystallogr.*, 2009, **42**, 339-341.
39. A. L. Spek, *Acta Crystallogr.*, 1990, **A46**, 194-201.
40. A. L. Spek, *J. Appl. Crystallogr.*, 2003, **36**, 7-13.
41. A. L. Spek, *Acta. Crystallogr.*, 2009, **D65**, 148-155.